Chin.J.Geochem.(2013)32:392–397
DOI: 10.1007/s11631-013-0647-x

The occurrence of gold in pyrite from the Liulincha gold ore belt, western Hunan Province, China

LI Zengsheng[1,2*], ZHU Xiaoqing[1], LU Huanzhang[1,3], and HAN Tao [1,2]

[1] *State Key Laboratory of Ore Deposit Geochemistry, Institute of Geochemistry, Chinese Academy of Sciences, Guiyang 550002, China*

[2] *University of Chinese Academy of Sciences, Beijing 100049, China*

[3] *University of Quebec at Chicoutimi, G7H 2B1, Canada*

[*] *Corresponding author, E-mail: lizengsheng@126.com*

Received March 3, 2013; accepted April 3, 2012

Abstract In this study, an electron microprobe analyzer (EMPA) was used to map the spatial distribution and the occurrence of invisible gold in pyrite from the Liulincha gold ore belt. EPMA data show that gold mainly occurs as submicroscopic-microscopic inclusions. From the contrast of the major guide elements of pyrite from the Liulincha gold ore belt and those from four hydrothermal-type gold deposits in the Jiaodong region, we can see the pyrites were formed in two stages: the pyrite from wall rock is mainly sedimentogenic, with simple structure; and the pyrite from ore body experienced early sedimentary process to late hydrothermal activity, the pyrite is regular in crystal form and exhibits fractured structure.

Key words occurrence of gold; pyrite; invisible gold; Liulincha gold ore belt

1 Introduction

The Liulincha gold ore belt is one of the major metallogenic belts in the Xuefeng mountains, western Hunan, China. A number of albite-quartz vein-type gold deposits have been discovered in this metallogenic belt, and the main gold-bearing minerals include quartz, albite and pyrite. Usually, the visible gold exists in albite and quartz, and "invisible gold' exists in pyrite. Gold contained in the structure of the common sulfide minerals and that present as discrete inclusions smaller than 1000 Å are collectively termed "invisible gold", not detectable by optical and scanning electron microscopy (Cook and Chryssoulis, 1990). "Invisible gold" appears to be preferentially concentrated in pyrite and arsenopyrite (Cook and Chryssoulis, 1990; Palenik et al., 2004; Saha and Venkatesh, 2002; Fleet et al., 1993; Sung et al., 1993; Mumin et al., 1994; Majzlan et al., 1994; Yang Sixue et al., 1998; Pals et al., Simon et al., 1999). Basically, there are two viewpoints on the occurrence state of "invisible gold" in sulfides: one is that the gold is present in solid solutions in pyrite and arsenopyrite, and the other is that the gold occurs as submicroscopic inclusions (Simon, 1999; Healy and Petruk, 1990; Hannington, 1995; Larocque and Hodgson, 1995; Wagner et al., 2007; Vikentyev, 2004; Arechart, 1993; Bortnikon, 2003). Palenik (2004) gave two possible forming mechanisms for submicroscopic inclusions: (1) Au exceeded its solubility limit in arsenian pyrite, thus causing it to be deposited as nanoparticles of native gold; and (2) exsolution of native gold from metastable arsenian pyrite was caused by a later event in the history of the deposit (Palenik, 2004). Reich (2005) thought that the As and Au contents of arsenian pyrites plot in a wedge-shaped zone with an upper compositional limit defined by the line $C_{Au}=0.02^{*}C_{As}+4\times10^{-5}$, indicating a maximum Au/As molar ratio of -0.02 (Reich et al., 2005). According to the gold content analysis of pyrite in the Liulincha gold mine belt, the average gold content reached 114.67×10^{-6} in fine-grained pyrite and 5.67×10^{-6} in medium-fine grained (The Headquarter of Chinese Armed Police, 1996), but there has been no direct evidence for the occurrence state of gold in the pyrite.

The study on the occurrence state of gold in pyrite is useful to guide prospecting, mineral deposit evaluation and improvement of gold extracting method. Electron probe microanalysis (EPMA) has become a main approach to study preliminary "invisi-

ble gold", because it has high resolution, can give element distribution map, the content of element, etc. Using an electron probe microanalyzer (EPMA), the author has investigated the distribution characteristics and concentrations of invisible gold at different spots in pyrites of various grain sizes, crystal forms, and paragenetic stages. The samples used in this study were collected from the Herenping and Tongshumian gold mines of the Liulincha gold ore belt.

2 Geological setting

The Liulincha gold ore belt is located in Wuqiangxi Town, Yuanling Country, Hunan Province. The gold ore belt is about 40 km in length, and contains more than ten gold deposits. Both two selected gold mines are of the auriferous quartz-albite vein type. Of the two, the Herenping gold mine has a long history, which was recorded in the Ming Dynasty. Also it is one of the four main gold mines in Hunan in the late Ming and early Qing dynasties (The Headquarter of Chinese Armed Police, 1996). (Fig. 1, location of the gold deposit).

The strata exposed in this area consist mainly of the Neoproterozoic Banxi Group Madiyi Formation. The lower segment of the Madiyi Formation is not exposed; the middle segment is mainly composed of mauve sericitic slate and mingled with greyish-green banded sericite slates; and the upper segment is composed of greyish-green thin sandy slate. Folds and faults are developed in this zone, and the auriferous albite-quartz vein is mainly restricted within the mauve sericitic slate in the middle Madiyi Formation, and controlled by interlay faults. Magmatic activities are generally weak in western Hunan, and no igneous rocks outcrop within or around the Liulincha gold ore belt.

By appearance, orebodies can be divided into bedded vein, stockwork and joint vein (or veinlet). The metallic minerals include native gold, pyrite, etc.; sphalerite, galena and tetrahedrite are found on the Au-concentrated position. The gangue minerals include quartz, albite, and minor amounts of sericite, calcite and chlorite. Wall-rock alterations are predominated by decolorization, silicification, pyritization, carbonatization and sericitization.

3 Samples and methods

Samples for this study were collected from the Herenping and Tongshumian gold mines of the Liulincha gold ore belt. The analysis was finished at the State Key Laboratory of Ore Deposit Geochemistry, Chinese Academy of Sciences. The equipment used in this study was EPMA-1600, which is high in stability and accuracy. Electron microprobe analyses (EDS and WDS) were carried out under the following conditions, accelerating voltage: 25 kV, and sample current, 10 nA.

4 Results and discussion

The pyrites were formed in two stages (Fig. 2).

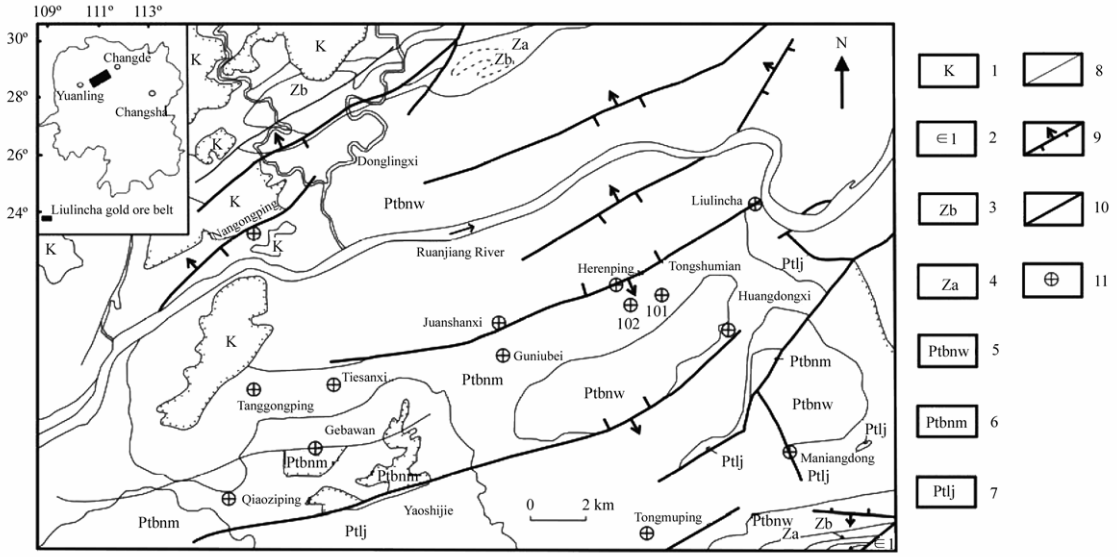

Fig. 1. Geological sketch map of the Liulincha gold ore belt modified from the reference (Wang Guoqiang, 2009). 1. Cretaceous; 2. the lower series of Cambrian; 3. the upper series of Sinian; 4. the lower series of Sinian; 5. Neoproterozoic Banxi Group Wuqiangxi Formation; 6. Neoproterozoic Banxi Group Madiyi Formation; 7. Neoproterozoic Lengjiaxi Group; 8. stratigraphic unconformity boundary; 9. reverse fault; 10. type-unknown fault; 11. gold deposit.

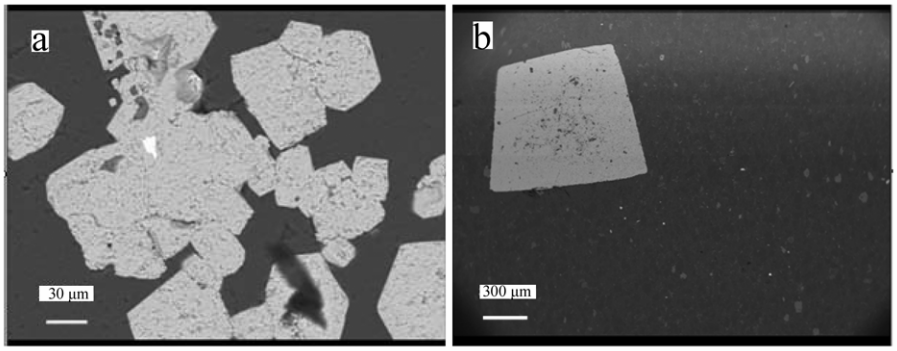

Fig. 2. BSE images of pyrites from the Liulincha gold ore belt. a. Pyrite from ore body; b. pyrite from wall rock.

The pyrites formed in the early stage of mineralization are euhedral and coarse grained, mostly cubic and porous; the pyrites formed in the late stage are medium-fine grained, anhedral and fractured. The gold concentrations are higher in fine-grained pyrites than in coarse-grained ones.

A lager number of submicroscopic-microscopic gold inclusions were found in this study (Fig. 3). These gold inclusions are distributed mainly on the edges of arsenian pyrite crystals or fractured fissures, of which the biggest one is 15 μm in scale and the smallest is less than 1 μm.

The contents of S and Fe in sedimentogenic pyrites are close to the theoretical values, or the content of S is slightly higher (Zhao Jiexin and Bao Mingxue, 2007). Under the condition of high temperature, the content of Te is higher in pyrite; and under the low temperature, the content of Se is higher, the content of S shows a little variation. The formation condition of pyrite can be distinguished by the values of w(S)/w(Se) and w(Se)/w(Te). Generally, the ratio of w(S)/w(Se) is more than 20×10^4 in sedimentogenic pyrite; the ratio varies between 1×10^4 and 2.67×10^4 in pyrite of hydrothermal origin. The ratio of w(Se)/w(Te)lies between 6 and 10 in magmatogenic pyrite; and the ratio is about 0.2 in pyrite of hydrothermal origin (Tong Jinggui et al., 2004). The contents of Co and Ni and the values of w(Co)/w(Ni) can indicate the deposit genesis. Generally, the ratio of w(Co)/w(Ni) is less than 1 in sedimentogenic pyrite; it is more than 1 in pyrite of hydrothermal origin.

Table 1 lists the mineral chemistry of pyrite by EMP.

(1) Pyrite from ore body: it is shown that the contents of S in pyrite from ore bodies are within the range of 51.103%–53.003%, those of Fe are within the range of 43.010%–46.184%, and those of S and Fe are lower than the theoretical values. That is because of the isomorphism of As, Co, Ni, Te, Au, Ag and so on, among which the content of As is highest. As has a great influence on the major component of pyrite, because As can substitute S easily.

Table 2 shows the contrast of the major guide elements of pyrite from the Liulincha gold ore belt and those from four the hydrothermal-type gold deposits in the Jiaodong region. The proportion of n(S)/n(Fe)>2 of pyrite from the Liulincha gold ore belt is 66%, which has the characteristics of the epithermal- or sedimentary-type gold deposits, and it is similar to that of pyrite in the hydrothermal-type gold deposits in Jiaodong. The average value of w(Co)/w(Ni) is less than 1, which shows a sedimentary-type pyrite. The average value of w(Se)/w(Te) is 0.53, it is similar to the value of the hydrothermal-type pyrite in Jiaodong, which shows that the pyrite is not normally sedimentary, whereas it has a close relationship with the hydrothermal process.

(2) Pyrite from wall rock: the contents of S are within the range of 51.085%–52.855%; and those of Fe, 44.376%–45.906%; both are lower than the theoretical values. The contents of As in pyrite from wall rock are lower than those of As from ore body, so the contents of Au are also relatively low. The value of w(Co)/w(Ni) is less than 1, so the pyrite may be sedimentogenic. From the backscattered electron images we can see that though the crystal form of pyrite from wall rock is good and the core is porous, it is likely that in the early growth period of pyrite silicic impurities are interfused.

Pyrites from the Liulincha gold ore belt generally contain a certain amount of As, which cause the contents of Fe and S to be deviated from the theoretical values. As viewed from backscattered electron images in combination with the spectrum data, it is concluded that the pyrite from wall rock is mainly sedimentogenic with good crystal form and simple structure; the pyrite from ore body experienced early sedimentary process to late hydrothermal activity, the pyrite has a regular crystal form and exhibites fractured structure.

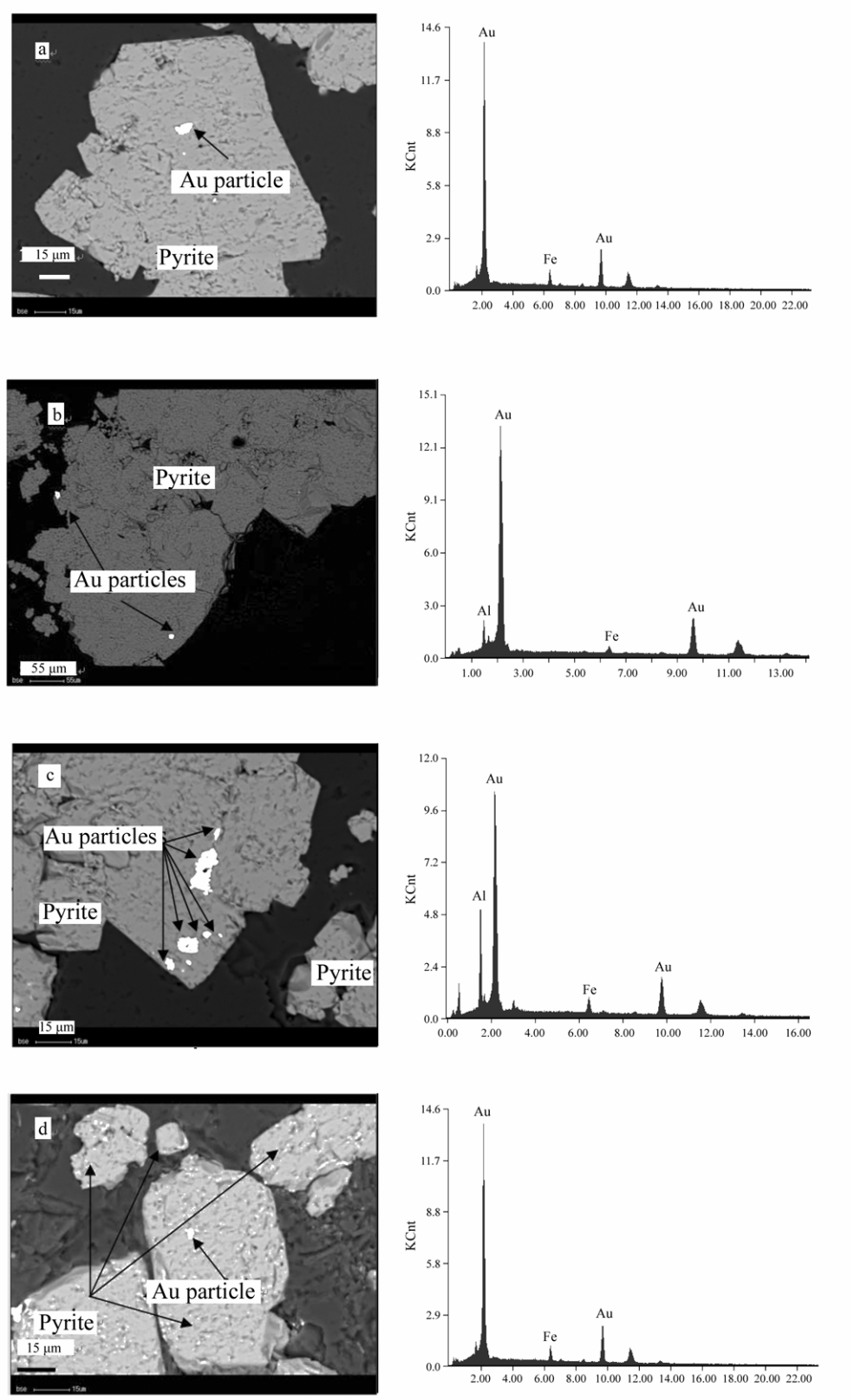

Fig. 3. Gold particles and energy dispersion spectra.

Table 1 Mineral chemistry of pyrite (EMP wt.%)

Sample No.	Test point	S	Fe	As	Co	Ni	Se	Te	Au	Ag	Total
Hrp-3 (ore body)	1	52.813	44.678	1.633	\	\	0.021	\	0.207	0.023	99.376
	2	51.866	44.226	1.993	\	0.043	\	0.077	0.087	\	98.292
	3	51.906	45.442	1.646	\	\	0.03	\	0.007	0.007	99.077
	4	52.933	43.010	1.694	\	\	\	0.018	0.007	\	97.662
	5	52.252	44.205	1.253	0.041	0.026	0.075	0.185	0.206	0.043	98.286
	6	51.895	45.887	1.125	\	0.037	0.001	\	0.010	\	98.954
	7	51.103	45.302	1.490	\	\	0.040	0.029	0.091	0.026	98.081
	8	51.410	45.561	1.997	0. 181	0.162	\	\	0.002	0.004	99.317
	9	51.381	44.799	1.740	\	0.044	0.015	\	\	0.056	98.035
Tsm-3 (ore body)	10	52.761	45.931	0.991	\	\	\	0.019	0.023	0.005	99.730
	11	53.003	45.942	1.043	\	\	\	0.015	\	0.010	100.093
	12	52.774	46.184	0.629	\	0.009	\	\	0.032	\	99.591
	13	52.882	45.607	0.760	0.029	0.020	\	\	\	\	99.298
	14	52.416	45.653	0.796	\	0.054	\	\	0.016	0.018	98.953
	15	52.716	45.875	0.853	\	0.058	\	\	0.029	0.015	99.547
Tsm-1 (wall rock)	16	52.029	45.373	0.658	\	0.058	\	0.002	0.016	0.006	98.142
	17	51.376	44.376	0.593	\	0.046	\	0.002	0.018	0.007	96.418
	18	52.855	44.663	0.641	\	\	\	0.026	0.030	0.055	98.269
	19	52.852	45.104	0.581	\	0.024	0.001	0.094	0.050	0.018	98.725
Hrp-1 (wall rock)	20	52.235	45.906	0.590	0.001	0.136	\	0.022	0.089	0.015	98.995
	21	52.212	45.273	0.486	\	\	\	\	0.075	0.004	98.050
	22	51.085	45.222	0.532	\	0.061	0.026	\	0.059	0.022	97.007
	23	52.760	44.570	0.579	\	\	0.086	0.043	0.092	\	98.135
Tsm-2 (wall rock)	24	52.403	44.924	0.611	0.041	0.076	\	0.018	\	0.023	98.095
	25	51.888	45.091	0.740	0.127	0.146	\	0.066	0.032	\	98.090
	26	52.044	45.548	0.591	0.002	0.092	\	\	\	0.008	98.284
	27	52.049	45.338	0.600	0.036	0.098	0.024	\	\	\	98.145
	28	52.481	44.576	0.639	\	0.071	\	0.032	\	0.008	97.809
Hrp-2 (wall rock)	29	52.483	44.972	0.590	0.056	0.135	\	\	0.032	0.015	98.282
	30	52.836	44.417	0.609	0.075	0.095	\	\	0.007	0.027	98.066
	31	51.669	44.539	0.577	0.123	0.111	0.007	\	0.096	\	97.122
	32	52.788	44.613	0.572	\	0.020	0.017	\	\	0.017	98.027

Note: Hrp. Herenping gold mine; tsm. T. ongshumian gold mine; \. no data.

Table 2 The comparison of some chemical typomorphic characteristics between pyrites from the Liulincha gold ore belt and those from gold deposits in the Jiaodong region

Deposit		W(trace element) (10^{-6})				*n*(S)/*n*(Fe)	w(Co)/w(Ni)	w(S)/w(Se)	w(Se)/w(Te)
		Co	Ni	As	Se				
Turbidite-hosted	Liulincha gold ore belt	167.33	302.00	13095.33	121.33	1.974–2.153, >2 (66%)	0.55 (average)	0.43×10^4	0.53
Hydrothermal filling type	Jinqingding gold mine	131.35	85.86	2576.00	4.89	>2 (64%)	2.83	13.6×10^4	0.43
	Xishan gold mine	81.50	54.30	689.00	1.70	most< 2	0.08–9.5 2.41 (average)	49.2×10^4	1.34
Hydrothermal metasomatic type	Sanshandao gold mine	77.24	23.33	7530.70	<1.00	>2 (60%) <2 (40%)	0.33–7.83 2.22 (average)	52.04×10^4	0.17
	Jiehe gold mine	365.00	277.40	14.99	100.00	2.008 (average)	1.3 (average)	0.5×10^4	0.10

5 Conclusions

(1) Gold in pyrites from the Liulincha gold ore belt occurs as submicroscopic to microscopic size gold particles that are occasionally present on the gold-bearing arsenian pyrite edges and in fissures.

(2) The pyrite from wall rock is mainly sedimentogenic, with simple structure; and the pyrite from ore body experienced early sedimentary process to late hydrothermal activity, and the pyrite is regular in crystal form and exhibits fractured structure.

References

Arechart G.B., Chryssoulis S.L., and Kesler S.E. (1993) Gold and arsenic in iron sulfides from sediment-hosted disseminated gold deposits: Implications for depositional processes [J]. *Economic Geology*. **88**, 171–185.

Bortnikov N.S., Cabri L.J., Vikentiev I.V. et al. (2003) Invisible gold in sulfides from modern pyrite chimneys [J]. *Geology Ore Deposits*. **45**, 232–245.

Cook N.J. and Chryssoulis S.L. (1990) Concentration of "invisible" gold in the common sulfides [J]. *Canadian Mineralogist*. **28**, 1–16.

Fleet M.E., Chryssoulis S.L., Maclean P.J., Davidson R., and Weisener C.G. (1993) Arsenian pyrite from gold deposits: Au and As distribution investigated by SIMS and EMP, and color staining and surface oxidation by XPS and LIMS [J]. *Canadian Mineralogist*. **31**, 1–17.

Hannington M.D., Tivey M.K., Larocque C.L., Petersen S., and Rona P.A. (1995) The occurrence of gold in sulfide deposits of the TAG hydrothermal field, mid-atlantic ridge [J]. *The Canadian Mineralogist*. **33**, 1285–1310.

Healy R.E. and Petruk W. (1990) Petrology of Au-Ag-Hg alloy and "invisible gold" in the Trout Lake massive sulfide deposits, Flin Flon, Manitoba [J]. *The Canadian Mineralogist*. **28**, 189–206.

Larocque C.L. and Hodgson C.J. (1995) Ion-microprobe analysis of pyrite, chalcopyrite and pyrrhotite from the mobrun VMS deposit in northwestern Quebec: Evidence from metamorphic remobilization of gold [J]. *The Canadian Mineralogist*. **33**, 373–388.

Majzlan J., Chovan M., Andras P. et al. (2010) The nanoparticulate nature of invisible gold in arsenopyrite from Pezinok (Slovakia) [J]. *Neues Jahrbuch Fur Mineralogie-abhandlungen*. **1**, 1–9.

Mumin A.H., Fleet M.E., and Chryssoulis S.L. (1994) Gold mineralization in As-rich mesothermal gold ores of the Bogosu-Prestea mining district of the Ashanti Gold Belt, Ghana: Remobilization of "invisible" gold [J]. *Mineral Deposita*. **29**, 445–460.

Palenik C.S., Utsunomiya S., Reich M. et al. (2004) "Invisible" gold revealed: Direct imaging of gold nanoparticles in a Carlin-type deposit [J]. *American Mineralogist*. **89**, 1359–1366.

Pals D.W. and Chressoulis S. (2003) Invisible gold and tellurium in arsenic-rich pyrite from the emperor gold deposit, Fiji: Implications for gold distribution and deposition [J]. *Economic Geology*. **98**, 479–493.

Reich M.R., Kesler S.E., Ursunomiya S. et al. (2005) Solubility of gold in arsenian pyrite [J]. *Geochimica et Cosmochimica Acta*. **69**, 2781–2796.

Saha I. and Venkatesh A.S. (2002) Invisible gold within sulfides from the Archean Hutti-Maski schist belt, Southern India [J]. *Journal of Asian Earth Sciences*. **20**, 449–457.

Simon G., Kesler S.E., and Chryssoulis S. (1999) Geochemistry and textures of gold-bearing arsenian pyrite, Twin Creek, Nevada: Implications for deposition of gold in Carlin-Type deposits [J]. *Economic Geology*. **94**, 405–422.

Sung Y.H., Brugger J., Ciobanu C.L. et al. (2009) Invisible gold in arsenian pyrite and arsenopyrite from a multistage Archaean gold deposit: Sunrise Dam, Eastern Goldfields Province, Western Australia [J]. *Miner Deposita*. **44**, 765–791.

The Headquarter of Chinese Armed Police (1996) *Geological of Woxi-type Stratabound Gold Deposit in Hunan Province* [M]. pp.18–47. Seismic Press, Beijing (in Chinese).

Tong Jinggui, Li shengrong, Xiao Qiyun et al. (2004) The chemical typomorphism genesis of the pyrites from the Zhongnancun black-rock-series [J]. *Geoscience*. **18**, 41–47 (in Chinese).

Vikentyev I.V., Yudovskaya M.A., Mokhov A.V., Kerzin A.l., and Tsepin A.I. (2004) Gold and PGE in massive sulfide ore of the Uzelginsk deposit, southern Urals, Russia [J]. *The Canadian Mineralogist*. **42**, 651–665.

Wagner T., Klemd R., Wenzel T., and Mattsson B. (2007) Gold upgrading in metamorphosed massive sulfide ore deposits: Direct evidence from laser-ablation-inductively coupled plasma-mass spectrometry analysis of invisible gold [J]. *Geology*. **35**, 775–778.

Wang Guoqiang, Peng Jiantang, Zhang Dongliang, Yang Jiehua, and Shen Nengping (2009) Mineralogy and geochemistry of albties from the Liulincha gold ore belt, western Hunan Province, China [J]. *Acta Mineralogica Sinica*. 29, 463–470 (in Chinese).

Yang Sixue, Blum N., Rahders E., and Zhang Zhenru (1998) The nature of invisible gold in sulfides from the Xiangxi Au-Sb-W ore deposit in northwestern Hu'nan, People's Republic of China [J]. *The Canadian Mineralogist*. **36**, 1361–1372.

Zhao Jiexin and Bao Mingxue (2007) Analysis on typomorphic characteristics and gold bearing properties of pyrite in Jiaojia gold deposit [J]. *Gold*. **9**, 19–23 (in Chinese).